

Digital Twin-enabled Task-driven UAV Communications Under Uncertainty

Bowen Wang, Yanjing Sun, *Member, IEEE*, Octavia A. Dobre, *Fellow, IEEE*, Long D. Nguyen, *Member, IEEE*, Trung Q. Duong, *Fellow, IEEE*

Abstract—Efficient task information interaction is the key to unmanned aerial vehicle (UAV) swarm collaboration. However, the driving force of both the spatial-temporal correlation and physical-virtual interaction has not been fully considered in existing works. In this paper, we aim to utilize the advanced digital twin technology to realize the efficient information interaction between the physical and virtual layers for UAV swarm collaboratively performing various tasks. Considering the driving force of both task correlation and transmission timeliness, the physical-virtual interaction link selection problem is formulated under uncertain estimation deviations in the form of interval number. To address this challenging problem, we first utilize the interval optimization for transforming the uncertain utility values to the certain preference orderings in matching theory, and then propose an interval rank-maximal matching algorithm to make predictive link selection based on unilateral preference information. Simulation results confirm that our proposed method can improve the interaction efficiency significantly under uncertainty.

Index Terms—Digital twin, unmanned aerial vehicle, matching theory, physical-virtual interaction, uncertain interval number.

I. INTRODUCTION

WITH the ability to adapt to complex terrain environments, unmanned aerial vehicle (UAV) swarm has been widely applied in various areas, such as environmental monitoring and emergency response [1]–[3]. To improve the efficiency of UAV swarm collaboratively performing complex tasks, it is crucial to facilitate the task-based information interaction. In [4], the authors utilized the Jaccard’s coefficient to model the relevance of task types among UAVs. Based on the Tobler’s First Law of Geography, the spatial-temporal correlation between the data extracted from the performed task and the task to be performed reflects the data availability [5]. Hence, how to leverage the spatial-temporal features of various tasks to drive the interaction remains to be explored.

B. Wang and Y. Sun are with China University of Mining and Technology, Xuzhou, 221110, China (e-mail: {bowenwang, yjsun}@cumt.edu.cn).

O. A. Dobre is with Memorial University, St. John’s, NL A1C 5S7, Canada (e-mail: odobre@mun.ca)

L. D. Nguyen is with Duy Tan University, Da Nang 550000, Vietnam (email: nguyendinhlong1@duytan.edu.vn).

T. Q. Duong is with Memorial University of Newfoundland, St. John’s, NL A1C 5S7, Canada, and also with Queen’s University Belfast, BT7 1NN Belfast, U.K. (e-mail: trung.q.duong@qub.ac.uk).

This work was supported in part by the National Natural Science Foundation of China (62101556), the Natural Science Foundation of Jiangsu Province (BK20210489), the National Science and Technology Major Project (2024ZD1004505), and the Fundamental Research Funds for the Central Universities (2021ZDPY0208). The work of T. Q. Duong was supported in part by the Canada Excellence Research Chair (CERC) Program CERC-2022-00109. The work of O. A. Dobre was supported in part by the Canada Research Chair Program CRC-2022-00187.

When the interaction direction is determined by task correlation, the transmission timeliness determines the feasibility. Considering the highly dynamic nature of network status, the direct transmission link between two UAVs may be intermittently connected [6]. To tackle this problem, both the real-time relay and data ferrying modes are utilized to improve the transmission performance [7]. However, due to the delay caused by waiting for UAV arriving at the appropriate position, the timeliness requirement is difficult to meet. By exploiting the rich computing resource at edge or cloud, the digital twin (DT) can help its physical object for raw data processing and analysis. In [8], the authors introduced three DT communication modes containing physical-to-physical (P2P), physical-to-virtual (P2V), and virtual-to-virtual (V2V) communications. Considering that the task information is simultaneously stored in the physical object and its DT, a natural question is raised, i.e., can we exploit the collaborative DTs for relaying the P2P communication through the high-rate physical-virtual interaction links?

With the above ideas in mind, the main challenge comes from the uncertain correlation and delay estimation deviations caused by trajectory offset, network variation, and data noise, etc. It is worthy mentioning that the probability distribution of delay or correlation parameter is usually difficult to obtain with small samples, while the fluctuation range depicted by the interval number is relatively easy to obtain through historical data [9]. With its ability to model uncertainty under unknown distribution and small samples, the interval optimization can transform the uncertain optimization problem containing interval parameters to a deterministic problem and solve it through heuristic algorithms [9]. However, the lack of performance guarantee restricts its application in uncertain environments.

As a powerful tool to model the beneficial relations among agents, matching theory has been widely applied to solve user selection problem in UAV communication networks [4], [7]. However, it is unrealistic to assume accurately predicted utility values in uncertain environments. In [10], the authors firstly transformed the uncertain utility values to the interval preference orders, and then used their expected values for bilateral matching. Due to lack of partial information after indirect transformation, it is difficult to compare any two intervals based solely on the expected preference values [9]. Based on the mean-variance criterion, we have proposed the stable matching model for solving the DT-enabled computation offloading problem under uncertainty [11]. However, the achieved ex-ante stability may be invalidated due to the bilateral uncertainty. In [12], the authors first proposed the

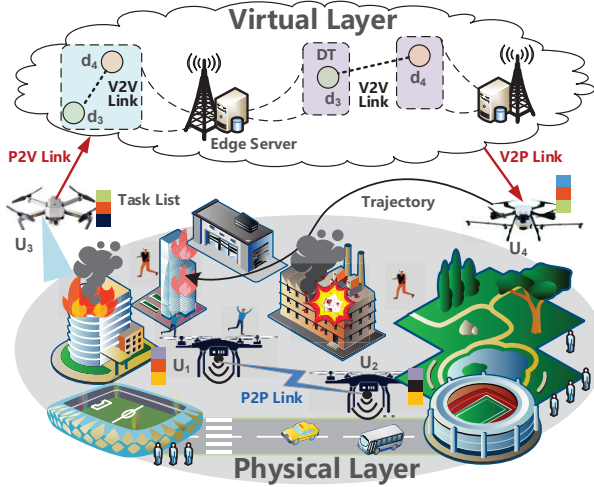


Fig. 1: Task-driven UAV physical-virtual interaction model. The blue icon represents the P2P interaction link. The black dashed line represents the V2V link through the I/O link when two DTs run on the same server, i.e., within the blue box, or otherwise through the wired link, i.e., between two purple boxes. The red line with arrow represents the P2V or V2P links in different transmission directions.

unilateral rank-maximal matching model that matches the maximum number of agents to their top-rank choice, second choice and so on, which offers a new way for circumventing the bilateral uncertainty. Considering that the assumption in [10] and our previous work [11] for the probability distribution of preference ordering values is difficult to satisfy in realistic scenarios, how to handle the unilateral matching without any prior knowledge about the uncertainty still needs to be explored.

By integrating the matching theory with interval optimization, the main contribution of this paper is a customized framework for physical-virtual interaction link selection with deviation ranges learned by DT. More specifically, we first propose a task-driven UAV physical-virtual interaction model, in which both the task correlation and transmission timeliness are considered as optimization objects while accounting for the uncertain estimation deviations in the form of interval numbers. Based on interval optimization, we transform the original uncertain optimization problem to a matching problem with certain preference orderings, and then propose an interval rank-maximal matching algorithm to balance the expected utility value and risk aversion degree of original optimization object. Simulation results confirm that our proposed method can improve the interaction efficiency under uncertainty.

II. SYSTEM MODEL AND PROBLEM FORMULATION

As shown in Fig.1, we consider a task-driven UAV physical-virtual interaction model, where a set of UAVs mounted with lightweight sensing and communication modules can collaborate with each other to execute various tasks such as temporary network recovery in dense hotspot areas, data collection for three-dimensional (3D) mapping and target detection in disaster areas [3]. Considering the periodic characteristics of these

tasks, the data extracted from the performed tasks such as traffic characteristic, service demand, and topographical features can improve the execution efficiency of similar tasks with close spatial-temporal distance. Besides, considering that the long-range P2P link may violate the timeliness requirement, the task-based information stored at the provider DT can share it with the requester DT through the V2V link, and then with the requester through the virtual-to-physical (V2P) link. Note that the transmission direction of P2V and V2P links are different, i.e., the former is from physical to virtual layer while the latter is in the opposite direction. It seems that the collaborative DTs constructed in the virtual layer act as relay for information interaction in the physical layer.

To facilitate the delay estimation in dynamic scenarios, the time period $\mathcal{T} \triangleq \{1, \dots, t, \dots, T\}$ is divided into cumulative T slots with sufficiently small length δ , within which the network status can be regarded as static [6]. In slot t , N UAVs can be divided into the set of information providers $\mathcal{U}^p(t) = \{u_i^p\}_{i=1}^{N_p(t)}$ and requesters $\mathcal{U}^r(t) = \{u_j^r\}_{j=1}^{N_r(t)}$. For u_i^p , its virtual twin d_i^p contains the completion time t_i^m and coverage c_i^m of the m -th task in the list of executed tasks $\mathcal{U}_i^e(t)$ before t . Similarly, the virtual twin d_j^r contains the scheduled execution time t_j^k and coverage c_j^k of the k -th task in the list of unexecuted tasks $\mathcal{U}_j^u(t)$ before t . Inspired by the relevance of task types in [4] and the spatial-temporal correlation in [5], the normalized task correlation can be estimated as

$$\tilde{\phi}_{i,j}(t) = \frac{\sum_{m,n \in |\mathcal{U}_i^e(t) \cap \mathcal{U}_j^u(t)|} \varpi a^{|t_i^m - t_j^k|} + (1 - \varpi) b^{-\ln \frac{|c_i^m \cap c_j^k|}{|c_i^m \cup c_j^k|}}}{|\mathcal{U}_i^e(t) \cup \mathcal{U}_j^u(t)|}, \quad (1)$$

where ϖ , a and b are weight factors ranging from 0 to 1, $|t_i^m - t_j^k|$ denotes the time distance, and $|c_i^m \cap c_j^k|$ and $|c_i^m \cup c_j^k|$ denote the overlap and union coverage of two areas, respectively. Similarly, $|\mathcal{U}_i^e(t) \cap \mathcal{U}_j^u(t)|$ and $|\mathcal{U}_i^e(t) \cup \mathcal{U}_j^u(t)|$ denotes the common and total task types, respectively. Considering the deviations between the scheduled and actual task information, the real correlation value can be represented by an interval number $\phi_{i,j}(t) = [\tilde{\phi}_{i,j}(t) + \Delta\phi_{i,j}^L, \tilde{\phi}_{i,j}(t) + \Delta\phi_{i,j}^U]$, where $\Delta\phi_{i,j}^U$ and $\Delta\phi_{i,j}^L$ denote the upper and lower deviations, respectively.

Considering the physical-virtual interaction opportunities brought by DT, we respectively introduce the transmission models of physical and physical-virtual interaction links.

1) *Physical interaction*: If the physical link quality is good enough, u_i^p can directly transmit task-based information to u_j^r through the P2P link. Herein, the orthogonal frequency division multiple access (OFDMA) scheme is utilized to realize non-interference transmission and each link is equally allocated with an orthogonal bandwidth B . Besides, we consider the free-space path loss model for the line-of-sight (LoS) dominant P2P link in air [4] and its predicted transmission rate in t can be given by

$$\tilde{R}_{i,j}^{P2P}(t) = B \log_2 \left(1 + \frac{P_i^p \tilde{g}_{i,j}(t)}{\sigma^2} \right), \quad (2)$$

where P_i^p denotes the transmission power of the i -th provider, and the channel gain $\tilde{g}_{i,j}(t) = \eta_0 l_{i,j}^{-2}(t)$ contains the power

gain η_0 under unit reference distance. Considering the rate variation across any two consecutive time slots, the transmission delay $\tilde{\tau}_{i,j}^{P2P}(t)$ can be estimated by the number of occupied slots $n_{i,j}$ if duration is small enough [6], i.e., $\sum_{t=1}^{n_{i,j}} \delta \tilde{R}_{i,j}^{P2P}(t) = s_i(t)$ and $\tilde{\tau}_{i,j}^{P2P}(t) = n_{i,j} \delta$, where $s_i(t)$ denotes the data size.

Due to external factors such as strong winds, the UAV will deviate from the preset trajectory, which gradually causes the estimation deviations in path loss, rate, and delay. Similarly, the real delay in form of interval number can be represented by $\tau_{i,j}^{P2P}(t) = [\tilde{\tau}_{i,j}^{P2P}(t) + \Delta \tau_{i,j}^{L,P2P}, \tilde{\tau}_{i,j}^{P2P}(t) + \Delta \tau_{i,j}^{U,P2P}]$.

2) *Physical-Virtual interaction*: If the P2P link quality is bad, the DT d_i^p can interact with d_j^r through the V2V link, and then with the requester u_j^r through the V2P link. There exists two cases for the V2V link establishment: 1) if both d_i^p and d_j^r are running on the same edge server, the V2V link can be established through I/O virtualization, 2) if d_i^p and d_j^r are running on the different edge servers [13], the V2V link can be established through a wired link between two servers [14]. According to [13], [14], the rate of virtual I/O or wired link remains unchanged in the transmission process, and the estimated V2V delay $\tilde{\tau}_{i,j}^{V2V}(t)$ can be calculated by $s_i(t)/\tilde{R}_{i,j}^V(t)$ for case 1, and $\alpha s_i(t) l_{i,j}^e / \tilde{R}_{i,j}^W(t)$ for case 2, where $\tilde{R}_{i,j}^V(t)$ and $\tilde{R}_{i,j}^W(t)$ denote the transmission rates of virtual I/O and optical-fiber link, respectively, $l_{i,j}^e$ is the distance between two edge servers, and α is a positive coefficient.

Similar to the P2P link, the delay of the V2P link from the server constructing d_j^r to its physical object u_j^r can be estimated by $\sum_{t=1}^{n_{j,j}} \delta \tilde{R}_{j,j}^{P2V}(t) = s_j(t)$ and $\tilde{\tau}_{j,j}^{P2V}(t) = n_{j,j} \delta$, where the transmission rate of the V2P link can be given by $\tilde{R}_{j,j}^{P2V}(t) = B \log_2(1 + P_j^v \tilde{g}_{j,j}(t) / \sigma^2)$. Herein, we consider a practical air-to-ground (A2G) channel model for V2P link, which is assumed to experience altitude dependent Rician fading and large-scale path loss [15]. Thus, the channel gain can be expressed as $\tilde{g}_{j,j}(t) = \eta_1 \tilde{l}_{j,j}^{-\alpha_j}(t) \Omega_j$, where η_1 is the channel gain parameter depending on average channel attenuation and antenna characteristics, \tilde{l}_j is the uncertain distance between d_j^r to its physical object u_j^r , α_j is the path loss exponent, and Ω_j represents the altitude dependent Rician fading following the weighted noncentral- χ^2 distribution with two degrees of freedom and $\mathbb{E}[\Omega_j] = 1$. Since this channel model is widely used for characterizing the A2G channel, the definition and parameter settings of probability distribution function, Rician factor and the angle-dependent path loss exponent can be referred to [15] for more details. Due to the network variation and trajectory offset, the delay of the V2V and V2P links should also be represented by interval numbers, namely $\tau_{i,j}^{V2V}(t) = [\tilde{\tau}_{i,j}^{V2V}(t) + \Delta \tau_{i,j}^{L,V2V}, \tilde{\tau}_{i,j}^{V2V}(t) + \Delta \tau_{i,j}^{U,V2V}]$ and $\tau_{j,j}^{P2V}(t) = [\tilde{\tau}_{j,j}^{P2V}(t) + \Delta \tau_{j,j}^{L,P2V}, \tilde{\tau}_{j,j}^{P2V}(t) + \Delta \tau_{j,j}^{U,P2V}]$. Considering the additivity of interval numbers [9], the transmission delay can be summarized by

$$\tau_{i,j}(t) = \begin{cases} \tau_{i,j}^{P2P}(t), & \text{Physical interaction} \\ \tau_{i,j}^{V2V}(t) + \tau_{j,j}^{P2V}(t), & \text{Physical-virtual interaction.} \end{cases} \quad (3)$$

As for the UAV energy consumption for executing the m -th task, we should consider its worst case through the minimum initial energy $E_i^{min}(t) = \tilde{E}_i(t) + \Delta E_i^{min}(t)$ and the maximum

energy consumption $E_i^{c,max}(m) = \tilde{E}_i^c(m) + \Delta E_i^{max}(m)$ to avoid the energy shortage during missions. Considering that the energy consumption for communications is orders of magnitude smaller than that for flight [16], we mainly focus on the energy consumption for propulsion and hovering, which can be estimated as $\tilde{E}_i^c(m) = p_i^P \tilde{\tau}_i^P(m) \delta + p_i^H \tilde{\tau}_i^H(m) \delta$, where p_i^P and p_i^H denote the propulsion power and hover power [11], $\tilde{\tau}_i^P(m)$ and $\tilde{\tau}_i^H(m)$ denote the durations for propulsion and hovering. Note that the durations are uncertain due to the trajectory offset caused by the wind and other physical factors.

To further measure different delay requirements of various task-based information, the transmission timeliness modeled by the inverted sigmoid-type function in [7] can be given by $\rho_{i,j}(t) = \exp\{-10 \exp[\kappa((\tau_{i,j}(t) - \tau_{i,j}^{th}))]\}$, where κ denotes the downward trend of the timeliness before the threshold $\tau_{i,j}^{th}$. To comprehensively factor the data availability and transmission timeliness into link selection, the utility value achieved by establishing an interaction link from u_i^p to u_j^r can be represented as the weighted sum of $\phi_{i,j}(t)$ and $\rho_{i,j}(t)$, i.e., $\nu_{i,j}(t) = \beta \phi_{i,j}(t) + (1-\beta) \rho_{i,j}(t)$, where ω is the weight factor and $\nu_{i,j}(t) \in [\nu_{i,j}^L(t), \nu_{i,j}^U(t)]$. Based on the above discussion, the optimization problem can be formulated as

$$\max_{\omega} \sum_{t=1}^T \sum_{i=1}^{N_p(t)} \sum_{j=1}^{N_r(t)} \omega_{i,j,t} \nu_{i,j}(t) \quad (4a)$$

$$s.t. \quad \phi_{i,j}(t) \geq \phi^{th}, \rho_{i,j}(t) \geq \rho^{th}, \quad (4b)$$

$$\sum_{i=1}^{N(t)} \omega_{i,j,t} \leq 1, \sum_{j=1}^{M(t)} \omega_{i,j,t} \leq 1, \forall t \in \mathcal{T}, \quad (4c)$$

$$E_i^{min}(t) - E_i^{c,max}(m) \geq E_i^{th}, \quad (4d)$$

where the binary variable $\omega_{i,j,t}$ determines whether or not to establish the interaction link between u_i^p and u_j^r , $E_i^{min}(t) - E_i^{c,max}(m)$ is the remaining energy after completing the m -th task in the worst case and E_i^{th} is the remaining energy threshold. The constraint (4b) indicates that both availability and timeliness should exceed the threshold values. The constraint (4c) indicates that one provider can only share information with one requester while one requester can only obtain information from one provider at a certain time slot due to the limited transmission capacity of UAVs. The constraint (4d) ensures that each UAV has sufficient energy to successfully return to the charging point after completing its mission. Note that the problem (4) is a NP-hard combinatorial optimization problem with uncertain interval parameters, and clarifying how to compare any two interval utility values is the precondition for solving (4). Next, we integrate the interval optimization with the matching theory for deterministic problem transformation and efficient solution.

III. INTERVAL MATCHING-BASED LINK SELECTION

By abstracting requesters and providers as applicants and posts, problem (4) can be transformed as the classic one-to-one matching model if the utility values are certain for preference ordering [12]. Hence, it is crucial to determine the order relations of utility values for matching.

Based on the interval optimization [9], the order relation of interval numbers can be determined by the mindpoint

$\nu_{i,j}^m(t) = (\nu_{i,j}^U(t) + \nu_{i,j}^L(t))/2$ without any prior knowledge of the probability distribution, i.e., the expected performance under uncertainty, and width $\nu_{i,j}^w(t) = \nu_{i,j}^U(t) - \nu_{i,j}^L(t)$, i.e., the sensitivity to uncertainty. It means that the order relation $\nu_{i,j}(t) >_{mw} \nu_{i',j}(t)$ can be determined if the conditions $\nu_{i,j}^m(t) > \nu_{i',j}^m(t)$ and $\nu_{i,j}^w(t) < \nu_{i',j}^w(t)$ are met simultaneously. However, it is difficult to maximize the expected performance while minimizing the sensitivity to uncertainty for risk aversion in practical solutions. By transforming the two objective functions into a single one, we redefine the order relation \succsim based on the weighted sum of the midpoint and width of the interval utility values, i.e., $\nu_{i,j}^s(t) = \lambda \nu_{i,j}^m(t) - (1 - \lambda) \nu_{i,j}^w(t)$ with λ as the weighting factor. Then, the relation $u_i^p \succsim_{u_j^p} u_{i'}^p$ indicates that u_j^p prefers u_i^p to $u_{i'}^p$ if $\nu_{i,j}^s(t) > \nu_{i',j}^s(t)$. In this way, we finally transform the uncertain optimization problem (4) to the deterministic problem, which can be represented as $\max_{\omega} \sum_{t=1}^T \sum_{i=1}^{N_p(t)} \sum_{j=1}^{N_r(t)} \omega_{i,j,t} \nu_{i,j}^s(t)$ with constraint $\phi_{i,j}^s(t) \geq \phi^{th}$, $\rho_{i,j}^s(t) \geq \rho^{th}$, and (4c), where $\phi_{i,j}^s(t)$ and $\rho_{i,j}^s(t)$ are the weighted sum of the midpoint and width of $\phi_{i,j}(t)$ and $\rho_{i,j}(t)$, respectively. Note that the mode selection problem coupled into problem (4) can also be solved by comparing the transformed utility values.

Since \succsim is just the ex-ante evaluation for the actual order relation, the bilateral matching, i.e., both providers and requesters have preference ordering over each other, may increase the inaccuracy in two-way selection. Hence, the unilateral matching when only requesters have preferences over providers would seem to be an effective way to reduce the bilateral influence. In this case, we redefine the interval matching model $\mathcal{M}(t)$ in slot t as a triple $\langle \mathcal{U}^p(t), \mathcal{U}^r(t), \succsim_{U^r} \rangle$. Considering that the ex-ante stability must be invalid when revealing the true preferences, focusing on maximizing the rank of matched provider in each requester's preference order is a more reasonable solution with only order relation information. According to [12], the signature of $\mathcal{M}(t)$ can be defined as an $N_p(t)$ -tuple $(x_1, x_2, \dots, x_{N_p(t)})$, where x_i denotes the number of requesters who are matching with their i -th choice in \succsim_{U^r} , and $N_p(t)$ is the largest rank that can be used. Then, we can say that $\mathcal{M}(t)$ with signature $(x_1, x_2, \dots, x_{N_p(t)})$ is greater than $\mathcal{M}'(t)$ with signature $(y_1, y_2, \dots, y_{N_p(t)})$, i.e., $\mathcal{M}(t) \succ \mathcal{M}'(t)$, if $x_i \geq y_i$ and $x_k < y_k$ for $1 \leq i < k \leq N_p(t)$ while $x_i > y_i$ at least once. Based on the above discussion, the interval rank-maximal matching represents the matching with the maximal signature under the interval order relations.

The key to solving this problem lies in matching as many requesters as possible to their top-rank, second-rank providers, etc. By abstracting the order relations as edges, i.e., the edge of rank i means that the connected provider is the i -th choice for the connected requester, we can invoke the maximum matching in the reduced graph with the set of edge of rank i to ensure that the obtained matching $\mathcal{M}(t)$ contains the most edges with higher ranks. Here, the matching model can be abstracted as a bipartite graph $\mathcal{G}(t) = (\mathcal{V}(t), \mathcal{E}(t))$, where $\mathcal{V}(t) = \mathcal{U}^p(t) \cup \mathcal{U}^r(t)$ denotes the vertex set, and $\mathcal{E}(t) = \mathcal{E}_1 \cup \dots \cup \mathcal{E}_{N_p(t)}$ denotes the ranked edge set. The edges that do not meet constraint (4b) have been deleted from $\mathcal{G}(t)$. Considering that one provider may be connected to more than

one requester from \mathcal{E}_i , we have to determine which one should be retained and then delete from $\mathcal{G}(t)$ the useless edges without prejudice to the final outcome. To this end, we introduce the concept of even, odd, and unreachable vertices.

Definition 1: If there exists an alternating path with even (odd) length from an unmatched vertex to v with respect to the maximum matching $\mathcal{M}(t)$, we call v an even (odd) vertex. Besides, if there are no such even (odd) length alternating path, we call v an unreachable vertex. In this way, the vertex set $\mathcal{V}(t)$ can be partitioned into the even vertex set E , odd vertex set O , and unreachable vertex set U .

Based on the graph structure of maximum matching, the authors in [12] proved a lemma for maximum matching. Herein, we utilize the lemma for algorithm design and the readers can refer to [12] for more details about the proof.

Lemma 1 ([12]): Some important properties about the sets E , O and U with respect to the maximum matching $\mathcal{M}(t)$ can be listed as follows: 1) E , O and U are pairwise disjoint and the same for any maximum matching of $\mathcal{G}(t)$, 2) each vertex in O is matched with the vertex in E and the vertex in U can only be matched within U . Hence, the size of maximum matching is $|O| + |U|/2$, and 3) the conditions that the vertex in E is matched with the vertex in $E \cup U$ and the vertex in O is matched with the vertex in $O \cup U$, will never happen for any maximum matching of $\mathcal{G}(t)$.

Based on **Lemma 1**, we can match as many requesters as possible to the providers ranked higher through augmenting and removing. For example, we first obtain the maximum matching $\mathcal{M}_1(t)$ with the E_1 , O_1 and U_1 in graph $\mathcal{G}_1(t) = (\mathcal{V}(t), \mathcal{E}_1(t))$. After removing all useless edges of rank 2 which are connected with those vertices in $O_1 \cup U_1$, and useless rank 1 edges that one end is in O_1 but the other is not in E_1 , we augment $\mathcal{M}_1(t)$ to obtain $\mathcal{M}_2(t)$ in $\mathcal{G}_1(t) = (\mathcal{V}(t), \mathcal{E}_1(t) \cup \mathcal{E}_2(t))$. Considering that the matched vertices in $\mathcal{M}_1(t)$ are still in $\mathcal{M}_2(t)$, the signature of x_1 may remain unchanged. This way, we can obtain the rank-maximal matching $\mathcal{M}(t)$ step by step. Given $\mathcal{G}_i(t) = (\mathcal{V}(t), \mathcal{E}_1 \cup \dots \cup \mathcal{E}_i(t))$, the interval rank-maximal matching based link selection (IRMLS) algorithm can be summarized in Alg. 1.

To prove that $\mathcal{M}(t)$ is rank-maximal with respect to $\mathcal{G}(t)$, we need to prove that the removed edges in Alg. 1 do not appear in any rank-maximal matching of $\mathcal{G}_{i+1}(t)$ and each element in the former signature remains unchanged after successive augmentations.

Lemma 2: For $1 \leq i < j \leq N_p(t)$, the signature of $\mathcal{M}_i(t)$ is the same as the first i elements in the signature of $\mathcal{M}_j(t)$.

Proof: Considering that all vertices matching in $\mathcal{M}_i(t)$ are also matched in $\mathcal{M}_j(t)$ after successive augmentations and all useless edges are removed from $\mathcal{G}'_j(t)$, all edges at rank smaller than or equal to i in $\mathcal{G}'_j(t)$ belong to $\mathcal{G}_j(t)$. Also, since $\mathcal{M}_i(t)$ is the maximum matching having achieved the maximal signature, $\mathcal{M}_j(t)$ must have the same edges of rank i as $\mathcal{M}_i(t)$.

Proposition 1: The rank-maximal matching in $\mathcal{G}_i(t)$ is also a maximum matching in $\mathcal{G}'_i(t)$.

Proof: We prove this lemma through induction hypothesis. When $i = 1$, all edges of $\mathcal{G}'_1(t)$ have the same rank, and maximizing the signature is the same as finding the maximum

Algorithm 1 Interval Rank-maximal Matching based Link Selection (IRMLS) Algorithm

- 1: **Phase 1:** Initialization
 - 2: Proceed to the next slot t . The DT predicts the uncertain task correlation and delay parameters for its physical object for link selection, and determine the preference orders based on the interval utility values. Construct the graph $\mathcal{G}(t)$ and the reduced graph $\mathcal{G}'_1(t) = \mathcal{G}_1(t)$ in DT layer.
 - 3: **Phase 2:** Matching
 - 4: **for** $i = 1$ to $N_p(t) - 1$ **do**
 - 5: Divide the vertex set $\mathcal{V}(t)$ into E_i , O_i and U_i for each rank i .
 - 6: Remove the useless edges of $\mathcal{E}_j(t)$ connecting vertices in $O_i \cup U_i$, $\forall j > i$, that are matched in any maximum matching of $\mathcal{G}'_i(t)$.
 - 7: Remove the useless rank i edges from $\mathcal{G}'_i(t)$ that one end is in O_i but the other is not in E_i , which do not appear in any maximum matching of $\mathcal{G}'_i(t)$.
 - 8: Update the reduced graph $\mathcal{G}'_{i+1}(t) = \mathcal{G}'_i(t) \cup \mathcal{E}_{i+1}(t)$ and obtain the maximum matching $\mathcal{M}_{i+1}(t)$ by augmenting $\mathcal{M}_i(t)$.
 - 9: **end for**
 - 10: **Return** the matching $\mathcal{M}(t) = \mathcal{M}_{i+1}(t)$ in t .
-

matching in $\mathcal{G}'_1(t)$. Assuming that the statement is true for i , we now prove it for the $(i+1)$ -th round. For any rank-maximal matching $\mathcal{N}_i(t)$ in $\mathcal{G}_i(t)$ and its signature (x_1, \dots, x_i) , the signature of $\mathcal{N}_{i+1}(t)$ can be represented as $(x_1, \dots, x_i, x_{i+1})$ based on **Lemma 2**. Besides, $\mathcal{N}_{i+1}(t)$ cannot involve any removed edges from $\mathcal{G}'_i(t)$ since $\mathcal{N}_i(t)$ is also a maximum matching in $\mathcal{G}'_i(t)$, which indicates that the removed edges in the i -th round do not appear in any rank-maximal matching of $\mathcal{G}_{i+1}(t)$. Thus, any rank-maximal matching in $\mathcal{G}_{i+1}(t)$ is contained in $\mathcal{G}'_{i+1}(t)$. Furthermore, assuming that the signature of maximum matching $\mathcal{M}_{i+1}(t)$ in $\mathcal{G}'_{i+1}(t)$ is $(x_1, \dots, x_i, y_{i+1})$ based on **Lemma 2**, the condition $x_{i+1} \geq y_{i+1}$ holds since $\mathcal{N}_{i+1}(t)$ is rank-maximal. Meanwhile, considering that any rank-maximal matching in $\mathcal{G}_{i+1}(t)$ is contained in $\mathcal{G}'_{i+1}(t)$ and that $\mathcal{M}_{i+1}(t)$ is a maximum matching in $\mathcal{G}'_{i+1}(t)$, $x_{i+1} \leq y_{i+1}$ also holds, then we can infer that $x_{i+1} = y_{i+1}$. Hence, $\mathcal{N}_{i+1}(t)$ is also a maximum matching in $\mathcal{G}'_i(t)$ and we can conclude that $\mathcal{M}_i(t)$ is rank-maximal with respect to $\mathcal{G}_i(t)$ for every $1 \leq i \leq N_p(t)$.

After proving the correctness, we now discuss the implementation issues of Alg. 1. In the initialization phase, we exploit the real-time prediction capability of DT for the estimation of task correlation and delay parameters. Since the probability distribution of estimation deviations is unknown in advance and difficult to obtain with small samples in complex dynamic environments, we only use the fluctuation range depicted by the interval number for preference ordering, which is relatively easy to obtain through learning from historical data in practice. Then, considering that the graph theory models are widely used for the simplification and analysis of different network structures in real word, the bipartite graph $\mathcal{G}(t)$

is constructed for characterizing network links with spatio-temporal changes, and dynamically depict network topologies in DT layer. Based on this, the link selection problem can be transformed to find the rank-maximal matching in $\mathcal{G}(t)$. In this way, the computational complexity can be reduced and thus our proposed method can better handle the dynamic and uncertain nature of UAV communication networks. Finally, we analyze the computational complexity of Alg. 1.

Complexity Analysis: In the initialization phase, the complexity for constructing graph $\mathcal{G}(t)$ is $\mathcal{O}(|\mathcal{E}(t)| + |\mathcal{V}(t)|)$. In the matching phase, the operations for vertex set partition and edge removal can also be finished in $\mathcal{O}(|\mathcal{E}(t)|)$. To obtain $\mathcal{M}_{i+1}(t)$, the Hopcroft-Karp algorithm will take $\mathcal{O}(\min(\sqrt{|\mathcal{V}(t)|}, |\mathcal{M}_{i+1}(t)| - |\mathcal{M}_i(t)| + 1)|\mathcal{E}(t)|)$ for augmenting $\mathcal{M}_i(t)$. Considering that the iteration number is bounded by $N_p(t)$, the overall complexity can be bounded by $\mathcal{O}(\min(N_p(t)\sqrt{|\mathcal{V}(t)|}, \mathcal{V}(t) + N_p(t))|\mathcal{E}(t)|)$. Note that as many edges have been removed by constraint (4b) and **Lemma 1**, the actual complexity is much lower than this bound.

IV. SIMULATION RESULTS

In this section, we consider that a swarm of UAVs are distributed in an area of size $(2 \times 2 \times 0.5)$ km³ with pre-determined trajectories according to the tasks. For the task model, there are 3 types of tasks and each task list records 2 recently executed tasks and 2 pending tasks. Besides, there are 20000 time slots with duration $\delta = 500$ ms, and each task period is within the range $[100, 500]$ s. The extracted data from executed tasks is with size $[10, 100]$ Mbits. Note that the task list will be updated after each task execution. For the communication model, the minimal and maximum values of value Rician factor related parameter are set to 5 and 15 dB, the probability distribution function, and the angle-dependent path loss exponent of A2G channel are set according to [15], the channel gain parameters of P2P link and V2P link are set to $\eta_0 = -20$ dB and $\eta_1 = -30$ dB, the transmission power is 0.1 W and 0.5 W for UAV and edge server, respectively, the channel bandwidth is 2 Mhz, the noise power density is -130 dbm/Hz, the virtual I/O and wired link rates are within the ranges $[0.5, 1.2]$ and $[0.1, 1]$ Gbps [13], [14], respectively. The estimation deviation range is $\pm 10\%$. For the energy model, the battery capacity is 2×10^5 J and 20% of the energy is set as the threshold. During the execution of the algorithms, the interaction request follows the Poisson process with arrival rate $N/2$ and the delay requirement follows the exponential distribution with mean 5 s. The threshold values ϕ^{th} and ρ^{th} are set to 0.3 and 0.5, while the weight factors are set according to [4], [9].

To evaluate the attained interaction performance, we compare the IRMLS with different benchmarks, including the rank-maximal matching only considering the P2P link (RMP), the bilateral matching (BM) algorithm [4] based on the estimated utility values, and the uncertain preference matching (UPM) algorithm [10] based on the expected preference values. Note that the complexity of the above mentioned algorithms is similar to that of IRMLS. Moreover, we use the ‘‘Exhaustive Search (ES)’’ based on the revealed global

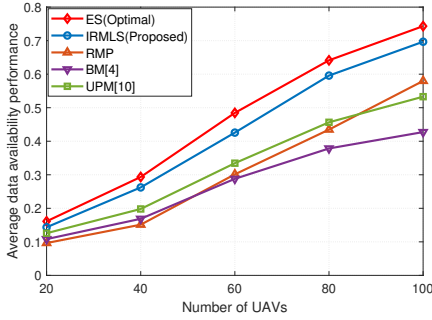


Fig. 2: Average data availability performance.

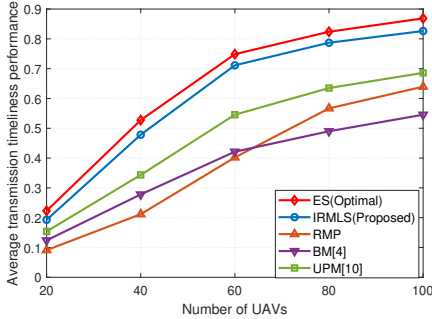


Fig. 3: Average transmission timeliness performance.

information in exponential time to give the upper bound performance.

Fig. 2 and 3 show the data availability performance, i.e., the task spatio-temporal correlation of obtained data, and the transmission timeliness performance versus the number of UAVs under uncertainty. Due to the high spatio-temporal separation between any two UAV nodes when the UAV number is small, the task spatio-temporal correlation is affected. In this situation, it is difficult to establish a physical-virtual link satisfying both requirements simultaneously, although the transmission timeliness requirement can be met in the virtual layer. As the density of UAVs increases, both performances are gradually improving, and the curve tends to flatten out when most requirements can be met.

Compared with other state-of-the-art algorithms, the IRMLS can always achieve the sub-optimal performances with proper complexity for both data availability and transmission timeliness. The reason are threefold. Firstly, by integrating the interval optimization into the matching theory, the IRMLS can handle the utility in the form of interval number. Secondly, the IRMLS focuses on the rank maximization and the unilateral preferences, which can reduce the inaccuracy of the traditional bilateral matching model. Finally, the physical-virtual interaction opportunities brought by DT further improve the interaction efficiency. Although our proposed IRMLS algorithm can fully utilize the DT to make predictable physical-virtual interaction link selection decision under uncertainty, there is still room for improvement in uncertainty quantification and complexity reduction. On one hand, further exploration of other information beyond interval width and center is needed for accuracy improvement. On the other hand, advanced data structure and approximate simplification approach should be integrated into the algorithm design for further reducing the

complexity.

V. CONCLUSION

By integrating the interval optimization with matching theory, we developed a novel interval matching framework for solving the physical-virtual interaction link selection problem under uncertain estimation deviations in the form of interval number. More specifically, we proposed an IRMLS algorithm with complexity bounded by $\mathcal{O}(\min(N_p(t), \sqrt{|\mathcal{V}(t)|}), \mathcal{V}(t) + N_p(t))|\mathcal{E}(t)|$, which can achieve enhanced data availability and transmission timeliness performances compared with other state-of-the-art algorithms. Although the interval optimization provide a new method to quantifying the mapping error of DT under small sample conditions, the lack of distribution information within the interval still leaves some room for improvement. In the future work, we aim to further explore effective ways to quantify uncertainty and enhance the practical value of our proposed uncertain optimization method in complex dynamic network environments.

REFERENCES

- [1] T. Do-Duy, L. D. Nguyen, T. Q. Duong, S. R. Khosravirad, and H. Claussen, "Joint optimisation of real-time deployment and resource allocation for UAV-aided disaster emergency communications," *IEEE J. Sel. Area. Comm.*, vol. 39, no. 11, pp. 3411–3424, Jun. 2021.
- [2] T. Bouzid, N. Chaib, M. L. Bensaad, and O. S. Oubbati, "5G network slicing with unmanned aerial vehicles: Taxonomy, survey, and future directions," *Trans. Emerg. Telecommun. Technol.*, vol. 34, no. 3, p. e4721, Dec. 2023.
- [3] K. Messaoudi, O. Oubbati, A. Rachedi, A. Lakas, T. Bendouma, and N. CHAIB, "A survey of uav-based data collection: Challenges, solutions and future perspectives," *J. Netw. Comput. Appl.*, vol. 216, p. 103670, Jul. 2023.
- [4] D. Liu, Z. Du, X. Liu, H. Luan, Y. Xu, and Y. Xu, "Task-based network reconfiguration in distributed UAV swarms: A bilateral matching approach," *IEEE/ACM Trans. Netw.*, vol. 30, no. 6, pp. 2688–2700, Jun. 2022.
- [5] L. Qiu, Z. Du, Q. Zhu, and Y. Fan, "An integrated flood management system based on linking environmental models and disaster-related data," *Environ. Modell. Softw.*, vol. 91, pp. 111–126, May. 2017.
- [6] D.-H. Tran, V.-D. Nguyen, S. Chatzinotas, T. X. Vu, and B. Ottersten, "UAV relay-assisted emergency communications in iot networks: Resource allocation and trajectory optimization," *IEEE Trans. Wireless Commun.*, vol. 21, no. 3, pp. 1621–1637, Aug. 2022.
- [7] D. Liu, Y. Xu, J. Wang, J. Chen, Q. Wu, A. Anpalagan, K. Xu, and Y. Zhang, "Opportunistic utilization of dynamic multi-UAV in device-to-device communication networks," *IEEE Trans. Cogn. Commun. Netw.*, vol. 6, no. 3, pp. 1069–1083, Apr. 2020.
- [8] Y. Wu, K. Zhang, and Y. Zhang, "Digital twin networks: A survey," *IEEE Internet Things J.*, vol. 8, no. 18, pp. 13 789–13 804, 2021.
- [9] C. Jiang and X. Han and H. Xie, *Nonlinear Interval Optimization for Uncertain Problems*. Springer Singapore, 2020.
- [10] D. Liu, Y. Yang, Y. Xu, X. Wang, and Y. Xu, "Uncertain preference matching-based relay selection and position adjustment in dynamic UAV systems," in *Proc. IEEE WCSP'20*, Nanjing, China, Oct. 2020, pp. 1170–1175.
- [11] B. Wang, Y. Sun, H. Jung, L. D. Nguyen, N.-S. Vo, and T. Q. Duong, "Digital twin-enabled computation offloading in UAV-assisted MEC emergency networks," *IEEE Wireless Commun. Lett.*, vol. 12, no. 9, pp. 1588–1592, Sept. 2023.
- [12] R. W. Irving, T. Kavitha, K. Mehlhorn, D. Michail, and K. Paluch, "Rank-maximal matchings." in *Proc. ACM-SIAM SODA*, New Orleans, LA, Jan. 2004, pp. 68–75.
- [13] W. Huang, M. J. Koop, Q. Gao, and D. K. Panda, "Virtual machine aware communication libraries for high performance computing," in *Proc. ACM/IEEE SC*, Reno, NV, Nov. 2007, pp. 1–12.
- [14] T. Liu, L. Tang, W. Wang, X. He, Q. Chen, X. Zeng, and H. Jiang, "Resource allocation in DT-assisted internet of vehicles via edge intelligent cooperation," *IEEE Internet of Things J.*, vol. 9, no. 18, pp. 17 608–17 626, Sept. 2022.

- [15] M. M. Azari, F. Rosas, K.-C. Chen, and S. Pollin, "Ultra reliable UAV communication using altitude and cooperation diversity," *IEEE Trans. Commun.*, vol. 66, no. 1, pp. 330–344, Jan. 2018.
- [16] J. Zhang, X. Hu, Z. Ning, E. C.-H. Ngai, L. Zhou, J. Wei, J. Cheng, and B. Hu, "Energy-latency tradeoff for energy-aware offloading in mobile edge computing networks," *IEEE Internet Things J.*, vol. 5, no. 4, pp. 2633–2645, Dec. 2018.